Detector Simulations at ARIANNA

DESY Summer Student Programme, 2018

Ida Torkjellsdatter Storehaug
Niels Bohr Institute, University of Copenhagen, Denmark

Supervisor
Anna Nelles

September 4, 2018

Abstract

The ARIANNA experiment seeks to observe neutrinos in the PeV range using a grid of antennas at the surface of the Ross Ice-shelf of Antarctica. The detector measures the coherent radiation produced at radio frequencies, from 100 MHz to 1 GHz, from particle showers generated by neutrino interaction in ice. In this project the data used is signal generated from air showers initiated from cosmic rays. As the emitted radio pulse passes through the antenna the signal is somewhat distorted. The antenna response is investigated, most notably the response to a change of signal arrival direction and group delay. It is found that the effect of group delay is smaller than expected, which supports the choice of an LPDA antenna in the experiment. The detector simulation is improved by adding simulation of background from human communication and the Galaxy.

Contents

1 Ultra-high Energy Neutrinos as a Probe into New Astrophysics

Up until recently, our way of observing the Universe has been through light. Now state-of-the-art methods, such as detection of gravitational waves and high energy neutrinos, are giving way to the new field of multi-messenger astronomy. A questions yet to be answered in astrophysics, is how cosmic rays are accelerated to high energies. Neutrinos with energy above the PeV range, so called ultra-high energy neutrinos, are predicted to be produced alongside cosmic rays. As neutrinos have a very small cross section and no charge, they rarely interact and travel in a straight line from the neutrino source. Thus by detecting cosmogenic neutrinos – neutrinos of cosmic origin – we can point straight back to the neutrino source, and perhaps discover the particle accelerators of the Universe. This is one of the motivations for detection of ultra-high energy neutrinos.

The same characteristics that make the neutrino an excellent probe into new astrophysics, also make detection difficult. As the energy of the neutrino increases, the cross section decreases, and detection requires enormous volumes of detector target material. The most common detection technique so far has been through observation of the Cherenkov light neutrinos emit in certain materials, a method that is used in IceCube and Super Kamikokande. However, to probe for neutrinos in the PeV range a much larger effective volume is needed. One can utilize the fact that high energy neutrinos does not only emit a light signal, but also a radio pulse (see Section 2.1 and 2.2). This radio pulse can be detected using antennas, a technology that is well-understood and cheap, enabling instrumentation of a much larger detector volume.

1.1 Radio Detection of Neutrinos: The ARIANNA Experiment

The Antarctic Ross Ice-Shelf Antenna Neutrino Array (ARIANNA) experiment is proposing the construction of an antenna array covering an area of 36 x 36 km^2 [1]. ARIANNA is to be installed in Antarctica, using the ice as target material. For radio frequencies the attenuation length in the cold ice of the South-pole is about 1 km, whereas the attenuation length for coastal ice is between 400 and 500 meters [1]. The stations of the array can thus be separated in such a way that a typical neutrino pulse will be measured by one station, maximizing the effective volume.

ARIANNA is proposed to be installed at the Ross Ice-shelf, where another characteristic of the ice can be utilized: the water-ice surface is very smooth and act as a mirror for the radio pulse signal initiated by the neutrino. The radio pulse in the ice is reflected back up towards the surface [1]. The antennas can therefore be placed on the surface, and by avoiding any drilling of deep holes in the ice, installation costs can be cut considerably.

To determine the properties of the neutrino each station will consist of multiple antennas. The experiment is currently in a pilot phase, functioning as the Hexagonal Radio Array (HRA), which has been taking data since 2014 [2]. HRA consists of 7 stations, each with four downward facing antennas. One of the stations is slightly altered and has two upwards facing antennas for rejection of air shower signals (Section 2.2). The set up is shown in Figure 1. When realized ARIANNA will have more than 1000 stations of similar design.

The ARIANNA will be using log-periodic dipole array (LPDA) antennas, sensitive between 100 MHz and 1 GHz. This range corresponds to a neutrino energy range between

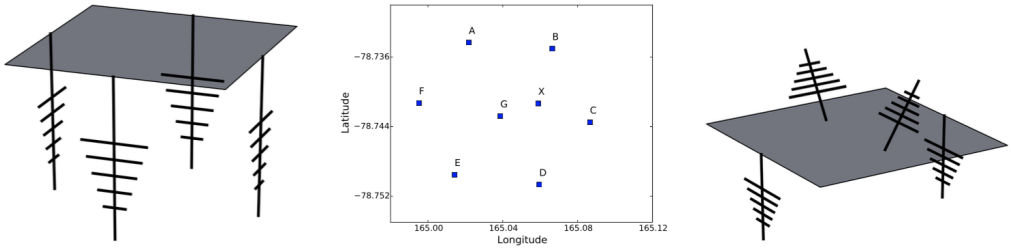

Figure 1: The HRA detector layout. The station at position X has two upward facing antennas for detection of air showers (right). The other 7 stations has four downward facing antennas for detection of neutrinos (left). From [3].

10^{16} eV and 10^{19} eV. The upper limit is set by the restrictions on the geometry of the antenna, the lower limit is caused by Galactic noise (Section 4.3).

2 Theory of Radio Emission

2.1 Radio Emission Initiated by Neutrinos

As a neutrino interacts with nuclei in the ice, a particle shower is created. For definiteness, consider a ν_e undergoing the reaction $\nu_e + N \rightarrow e + N'$. The neutrino transfers most of its energy to the electron, which builds an increasing shower of e^+e^- pairs. The positrons annihilate with electrons in the ice, whereas the electrons are swept with the shower due to Compton scattering. A charge imbalance develops: a negatively charged shower front and a positively charged trail. An electric field is produced by this net charge. As the shower is developing with time, a pulsed radiation with wavelengths in the radio frequency range is emitted. The phenomena is called the *Askaryan effect*.

Ice has a refractive index of $n > 1.0$, so the shower will propagate with a velocity of c, whereas the emission will propagate with a velocity of $v = c/n$. The geometrically shortest distance is therefore not the fastest path of propagation. As a result the pulsed emission will propagate with the shower for some distance before it deviates from the shower axis. This is analogous to Cherenkov radiation, and the experimental signature is also similar: a detected ring of radiation. This signature is caused by the fact that pulses emitted at every moment of time as the shower front propagates thorough the ice is added constructively in the Cherenkov angle. In the center of the shower the interference will be destructive and little or no radio emission will be detected.

2.2 Radio Emission Initiated by Cosmic Rays

When a cosmic ray hits a particle in the atmosphere a cascade of ionized particles and electromagnetic radiation is created. This cascade is called an air shower. The radio emission from an air shower is created by the Askrayan effect. There is however a difference in the Molière radius in ice and air, which is experimentally of great importance. In ice the Molière radius is approximately 10 cm, whereas in air it is $\mathcal{O}(1m)$. The shower front will be of the same depth as the Molière radius. To be emitted coherently the pulse must have a wavelength longer than the depth of the shower front. Thus, the wavelengths of

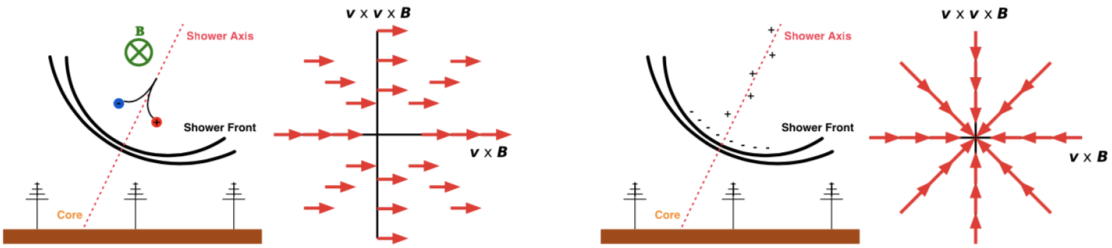

Figure 2: Left: Model of the geomagnetic emission. Right: Model of the Askaryan emission. From [4]

coherent pulses will be shorter in ice than in air. Higher frequency signals can therefore be detected in ice than in air. For air showers the emission is coherent for frequencies below 100 MHz [4].

Only 1% of the radiated power of air showers is caused by the Askaryan effect [4]. The main effect causing radio emission from air showers is due to the geomagnetic field: the trajectories of the secondary electrons and positrons in the cascade are bent in opposite direction in the magnetic field, creating an electric field. Because of the time dependency of the shower, a radio pulse is emitted. Both effects are illustrated in Figure 2. The emitted radio pulse is a superposition of the two emissions. Note that the two emissions have different polarizations. The geomagnetic emission is linearly polarized in the direction of the Lorentz force. The Askaryan emission is again linearly polarized, but the field vectors are pointing towards the shower axis. The superposition of the polarization leads to an asymmetry in the received amplitude depending on observer position, as is investigated in Section 3.2.

Pulsed emission from air showers has been found and studied in the pilot phase of ARIANNA. The radio emission from air showers are the main background to neutrino detection in ice. However, this can be suppressed using upward facing antennas in each station, which will trigger on radio emissions from air showers.

3 Methodology of Project

The emitted radio pulse from neutrino interaction or air showers is in the order of ten nanoseconds. However, as the signal passes through the detector, consisting of an antenna, an amplifier and a digitizer, the signal is somewhat distorted. The left plot of Figure 3 is a plot of the pulsed radio emission from a Monte Carlo generated air shower at a given position/station. As can be seen by the right plot of Figure 3, the shape and amplitude of the signal is changed as it passes through the detector. In this case the detector is simulated as a simple bandpass filter.

In my project I have investigated how different effects change the shape and amplitude of the detected signal. I have concentrated on three effects: change of position, group delay and background.

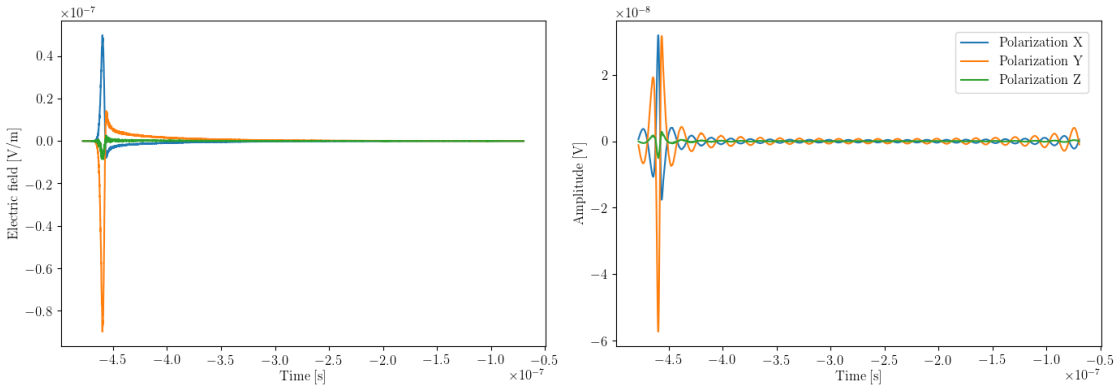

Figure 3: Left: Pulsed emission from a MC generated air shower (CoREAS) as a function of time. Right: The detected signal as a function of time.

3.1 The Data Used

I have focused on detection of air showers. Air showers are the background of neutrino detection in ARIANNA. However, it is also the calibration signal, making better knowledge on the physical behaviour of air shower important. The Monte Carlo simulations of air showers are done in CoREAS [5]. Studies have shown that the energy dependence, the height of the shower and the signal distribution on ground are reproduced with deviations of less than 10% using CoREAS [2].

Each datafile corresponds to one generated air shower. There are 160 stations in the simulation, and each data element is the electric field at a given moment at a particular station. The MC is constructed in such a way that the air shower is always in the centre of the station array.

3.2 Antenna Theory

As the electric field, $\vec{E}(t)$, hits the antenna, the antenna responds and a voltage $V(t)$ is generated. The mapping between the voltage response $V(t)$ and the electric field $\vec{E}(t)$ is represented by the vector effective length (VEL) $\vec{H}(t)$ of the antenna [6]. Of course, to understand how the signal changes as it passes through the detector, we must understand the antenna response.

For antenna calculations it is convenient to choose a spherical coordinate system, with the antenna in origo, in which the electric field of a plane wave arrives from a given direction (θ, ϕ) and is contained in the plane spanned by the unity vectors $\vec{e}_\theta$ and $\vec{e}_\phi$. Thus the electric field consists of two independent polarization directions which vary as a function of time:

$$\vec{E}(t) = \vec{e}_\theta \vec{E}_\theta(t) + \vec{e}_\phi \vec{E}_\phi(t) \tag{1}$$

The VEL of the antenna $\vec{H}(t)$ is also a two component vector in the antenna based coordinate system. The voltage response in the antenna is defined as $V(t) = \vec{H}(t) * \vec{E}(t)$, where $*$ marks the convolution transform. The convolution theorem allows to perform the convolution of functions as point wise multiplication of their Fourier transforms: $V(\omega) = \vec{H}(\omega) \cdot \vec{E}(\omega)$, where $\omega = 2\pi f$. Thus it is much more convenient to express both the electric field and the VEL as functions of frequency. This can be done using a Fourier transform.

The VEL at a given frequency, $\vec{H}(\omega = \omega_i)$ is a complex function:

$$\vec{H} = \vec{e}_\theta |H_\theta| e^{i\varphi H_\theta} + \vec{e}_\phi |H_\phi| e^{i\varphi H_\phi} \tag{2}$$

The absolute value of each component is then the amplitude, the effective length, or the gain. We can see that the gain of the antenna is dependent on the arrival direction of the signal. During this project I scanned over different arrival directions to investigate how the antenna response varies with arrival direction. Results is shown in Section 4.1.

3.3 Effects of Group Delay

As can be seen from eq. 2, $H(\omega)$ has a phase component, and a phase shift is cause by a delay in the system. However, in addition to a phase shift we also have a group delay. When passing through the antenna and amplifier, all frequency components of a signal are delayed. The signal delay will be different for the various frequencies: in ARIANNA specific systems high frequencies will be less delayed than low ones. As a result a signal consisting of multiple frequency components will be smeared out. It is defined as the negative response of the phase response:

$$\tau(\omega) = -\frac{d}{d\omega} e^{i\omega}$$

The ideal system would have no group delay, meaning that all frequency components experience the same delay as they pass through the detector. However, this is impossible to achieve. The detector simulation has not included group delay previously, and we want to investigate the effect of introducing group delay. As the group delay causes the signal to be smeared, the hypothesis is that when introducing group delay the maximum amplitude of the signal will decrease. To keep the same signal strength, one must therefore increase the gain of the antenna.

A parametrization of the group delay is obtained from measured data, where two antennas are connected in a loop to a network analyser. One antenna transmits a signal, and the other receives it, and the two signals are compared to quantify the difference. Then one antenna is moved around to see how the group delay varies with arrival direction. The «frontlobe»-model is a parametrization of the measured group delay when the signal arrives from the front, «backlobe» is the group delay parametrization when the signal arrives from the back, and «sidelobe» is from the side. A «theoretical» model, not based on measured antenna response, was also included.

For each model it was necessary to find how the maximum amplitude of each signal depends on the gain. For each signal the maximum amplitude was found, and the distribution of several signals plotted (Figure 4). The error on the bin count is taken to be Poission.

When the gain is increased or decreased the shape does not seem to change, though the peak is moving to higher amplitude maxima with increasing gain, as is to be expected. A simple calculation of the mean is done. As the distribution is not Gaussian, the error on the mean is set to be the standard deviation of the distribution. The mean of each distribution was found for several different gain values. The gain has a θ and ϕ component, but in this case if was deemed sufficient that they increased with equal amount during each iteration. Results are shown in Section 4.2

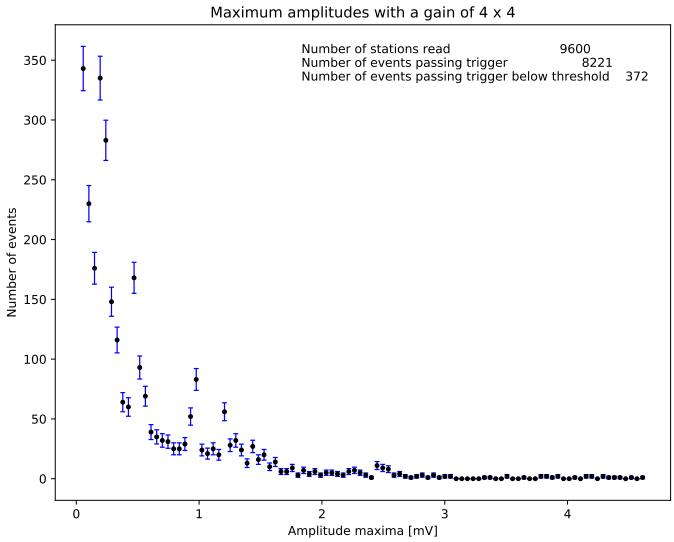

Figure 4: The distribution of signal voltage maxima at a fixed gain of 4.

3.4 Simulation of Background

As we have seen there are several advantages of radio detection. However, a major disadvantage is the level of background in a radio experiment. A typical background spectrum can be seen in Figure 5. The overall shape of the spectrum is caused by astronomical background, from Galactic steady-state emission and solar flares. At ARIANNA, a bandpass filter is implemented below 50 MHz to remove some astronomical background. However, the most significant source of background is human communication, such as air traffic control and walkie talkies.

Given that the backgrounds are known, one can imagine subtracting the background from the measurement. However, in case of substantial background the detector might saturate. Experimentally, narrowband filters can be a solution. If ARIANNA is to be

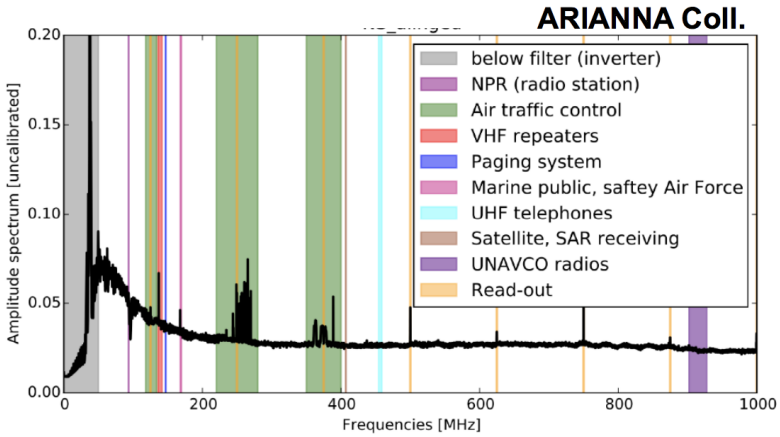

Figure 5: Background spectrum for ARIANNA

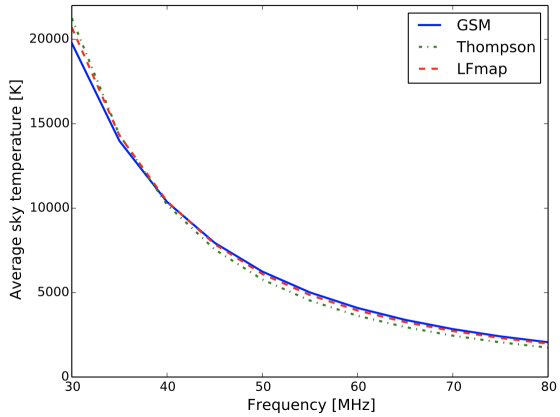

Figure 6: Average full sky temperature as a function of frequency [7]

used as a detector for air showers, one needs to have better knowledge of these sources of background. The present simulation does only contain a generic white noise (Figure 11). An objective of my project has been to simulate human made sources and Galactic background, to be combined with generic noise.

In simulation background is added to the signal. This can be done either in the frequency domain or in the time domain. When simulating human communication I chose to do this in frequency domain, as communication is often defined by the radio frequency. Using background data measured at HRA I found some typical frequency for narrowband communication by fitting Gaussian functions to peaks in the measured frequency spectrum.

Communication usually happen by either frequency modulation (FM) or amplitude modulation (AM). The simulation includes FM by sampling the background frequency from a normal distribution. The width of the Gaussian is found from a fit to data, to be around 0.05 MHz. The sampled frequency is used to generate a sinusoid wave. The period of the sinusoid is defied by the sampling rate and sampling number of the signal. In contrast to white noise, which is caused by effects of the antenna and therefore must be added to the signal after conversion from electric field to measured voltage, the narrowband background must be added as a electric field, with three polarization. The simulation constructed such that the user can define the power of the signal in three polarizations.

The Low Frequency-Array (LOFAR) has done research on models that interpolate to radio frequencies for Galactic background radiation. In the *LFmap* model the sky temperature can be described by a power law $T(\nu) \propto \nu^{-\beta}$, where the index β depends on frequency and observed direction [7]. However, it is found that this is consistent with all-sky temperature data sets. The model prediction for average sky temperature is read from a published plot (Figure 6). A fit to the model result in the value of $\beta = 2.41$ and $c = 10^{7.88}$. The received power spectral density is a function of the Rayleigh-Jeans law B, which is a approximation of the radiance at a given temperature at frequencies below 10^9 MHz [7]:

$$S_\nu = \int_\Omega B d\Omega = \frac{2k_B}{c^2}\nu^2 \int_\Omega T d\Omega = \frac{2k_B}{c^2}\nu^2 \int_\Omega 10^{7.88}\nu^{-2.41} d\Omega \tag{3}$$

Assuming full half-sphere sky view, we have a power spectral density of $S_\nu = 2\pi \cdot$

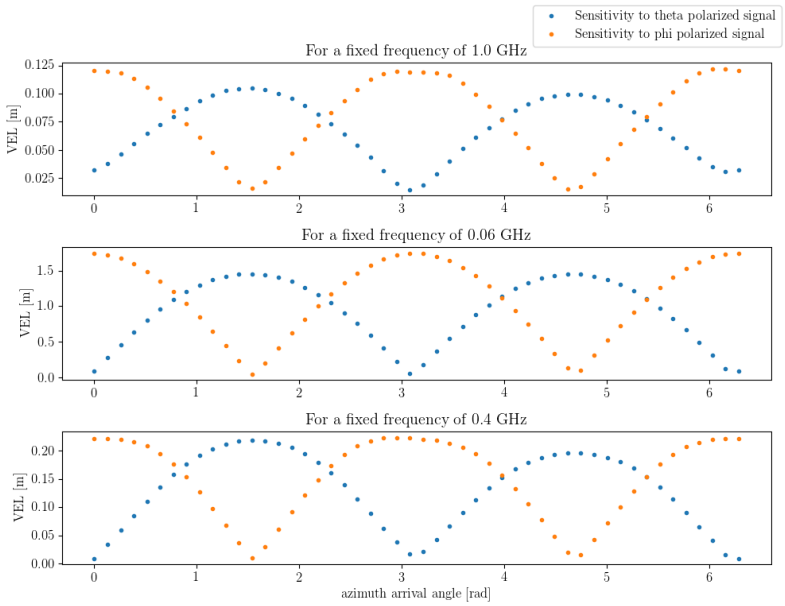

Figure 7: Plot showing the antenna response for various zenith arrival directions, at a fixed azimuth arrival direction of 180 degrees.

$\frac{2k_B}{c^2}\nu^2\omega 10^{7.88}\nu^{-2.41}$. It can be derived that the power spectrum density is related to the Fourier transform by:

$$S_\nu = \frac{2\Delta t|\tilde{X}_j|^2}{(N-1)} \tag{4}$$

where Δt is the sampling rate and N is the number of samples. $|\tilde{X}_j|$ is the amplitude of the Fourier transform in time domain. To get the full Fourier transform we can multiply with a random complex phase, $e^{\theta i}, \theta\epsilon[0, 2\pi]$, giving: $\tilde{X}_j = |\tilde{X}_j] \cdot e^{i\theta}$. The galactic radio emission can then be added to the signal. We can assume that the Galactic background is equaly polarized in all directions.

4 Results and Discussion of Results

4.1 Directivity of the Detected Signal

As can be seen from eq. (2) the VEL of the antenna depends on arrival direction of the signal, given in zenith, θ, and azimuth, ϕ, angle. To investigate the antenna response I first fixed the azimuth angle to π radians, and scanned for zenith arrival angles between 0 and 2π. This was done for three different radio frequency signals: 400 MHz, 600 MHz and 1 GHz. The result is plotted in Figure 8. I then repeated the exercise, this time for a fixed zenith angle of 30 degrees and scanning over azimuth arrival directions between 0 and 2π. The result is plotted in Figure 7.

For a fixed zenith angle, Figure 7, we observe that when the antenna is parallel to the ϕ-polarized part of the signal, at an azimuth angle of 0, π and 2π, it will be maximally

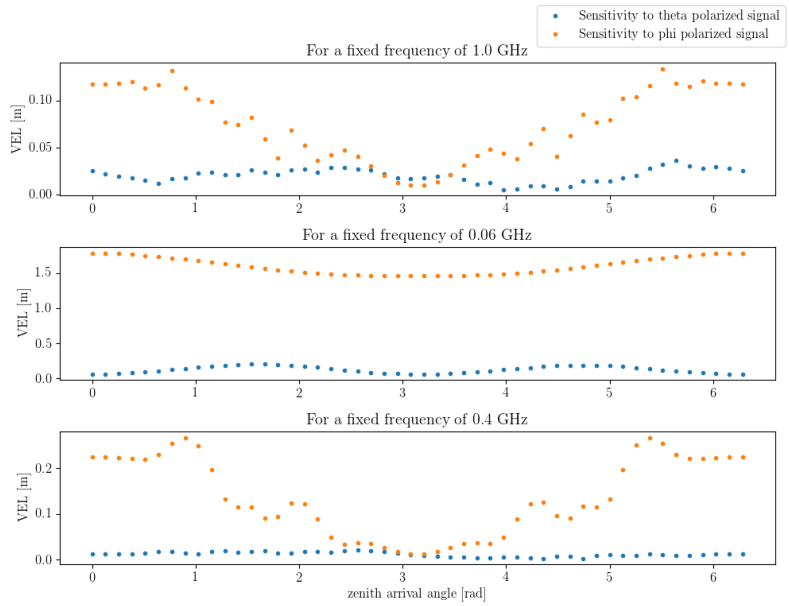

Figure 8: Plot showing the antenna response for various azimuth arrival directions, at a fixed zenith arrival direction of 30 degrees.

responsive to the ϕ-polarized signal. When the antenna is perpendicular to the ϕ-polarized signal part of the signal, at an azimuth angle of $\pi/2$ and $\pi/4$ it will not be sensitive to the ϕ-polarized signal at all. However at these positions the antenna will be maximally sensitive to the θ-polarized part of the signal. We can also se that the VEL, related to the gain of the antenna, is dependent on the frequency of the signal. In this case the signal will be more amplified at 600 MHz, than at 400 MHz and 1 GHz.

The same dependency between VEL and frequency is observed at a fixed azimuth angle (Figure 8). One does not observe the same periodic behaviour of the antenna response. As expected, the antenna is minimum sensitive to both polarizations when the signal has an arrival direction from the centre of Earth.

4.2 Including Group Delay Has Little Effect on the Gain

The mean maximum amplitude for different group delay parametrizations are plotted in Figure 9. For all models the mean maximum amplitude seem to increase linearly with increasing gain. Linear fit values can be seen in Figure 9. All fits have a χ^2 p-value of 1, which is caused by the fact that the error on the mean is taken to be the standard deviation. Therefore the error increases with higher gain, as the distribution becomes more smeared out. The number of events above trigger level increases by increasing gain, as one would expect.

The theoretical group delay model is an approximation, and from the ratio plot in Figure 9 we can see that theoretically 40% of the signal will be lost at a given gain. That will mean that you have to increase the gain by 40% to measure the same strength of signal with a theoretical group delay, independent of the gain of the antennas used. However, the models based on data show a smaller effect of 10-15%.

The result is of importance when considering which type of antenna to use in ARI-

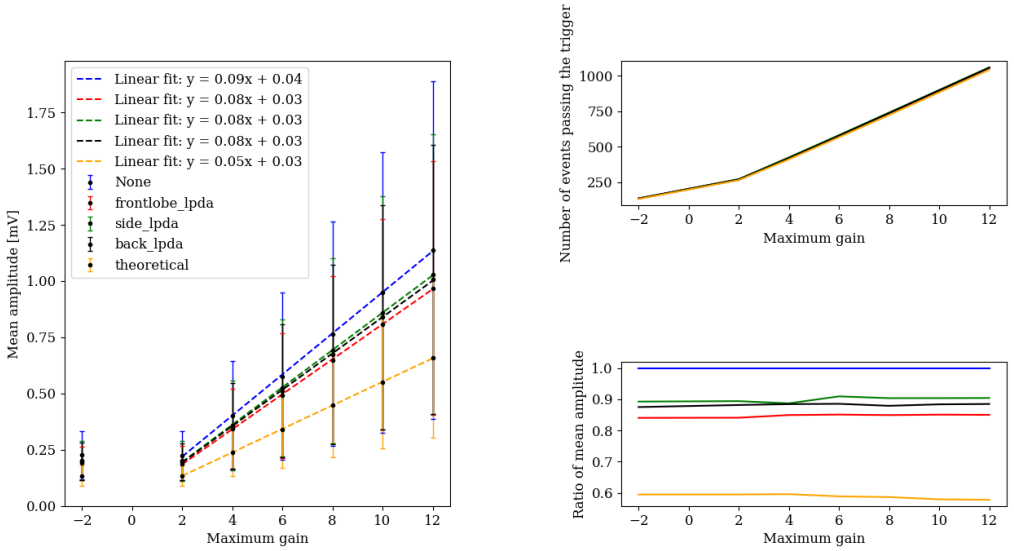

Figure 9: Left: The mean amplitude is likely to increase linearly with gain. Fit values are shown in the legend. Every fit has a χ^2 p-value of about 1. Upper right: The number of events above trigger level increases by increasing gain and is independent of group delay model. Lower right: Ration between no group delay and group delay models.

ANNA. The LPDA antenna used in HRA has a high group delay, but a maximum gain of 6. A dipole antenna would have little or no group delay, but a maximum gain of about 2. My result show that you would have a better signal with a gain of 6, even tough the group delay effect is reducing your signal by 10-15%, than you will have with a gain of 2 and no group delay. In this regard, the dipole antenna has no substantial advantage over the LPDA antenna.

4.3 Simulation of Narrowband Background

The effect of different type of simulated background is shown in Figure 10, 11 and 12. The user can add different types of background to the signal by calling the module for background simulation several times.

5 Conclusion

The main task of this project has been to build upon and improve ARIANNA detector simulation. An updated version of the simulation can be found in the Github repository [8]. For the antenna simulation effects of signal arrival direction has been in investigated. It has been found that effects of group delay lead to a 10-15% decrease of signal, a result that supports the use of LPDA antennas, where the high gain compensates for more group delay.

The ARIANNA simulation already includes a generic simulation of white noise. A simulation of background caused by narrow band, often radio communication, was added.

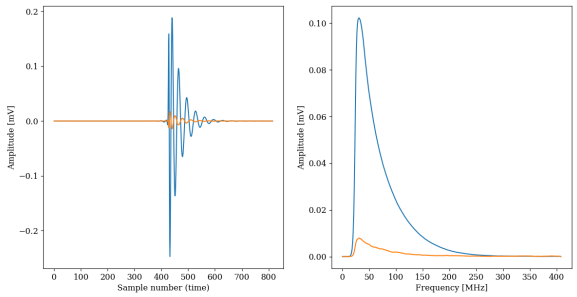

Figure 10: Signal with no noise added in time domain (left) and frequency domain (right).

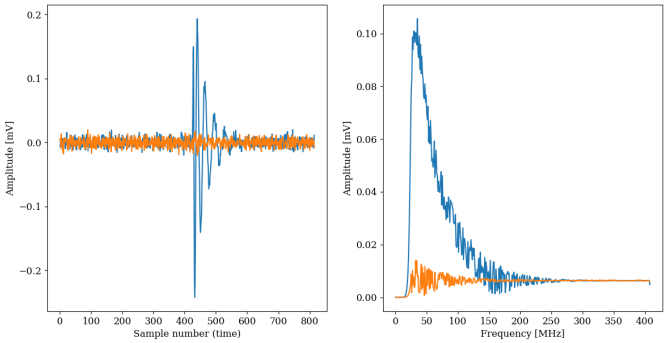

Figure 11: Signal with white noise added in time domain (left) and frequency domain (right).

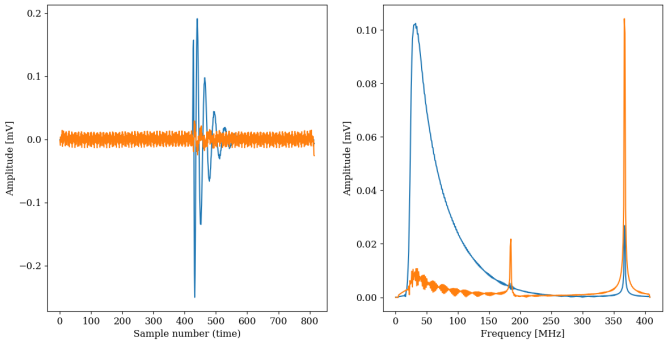

Figure 12: Measured signal with two radio wave background at 450 MHz (typical frequency for walkie talkies) and 226 MHz (generic air plane communication frequency). The first signal has a power of 0.1 MHz in all polarizations, whether the latter has a power os 0.01 MHz in all polarizations.

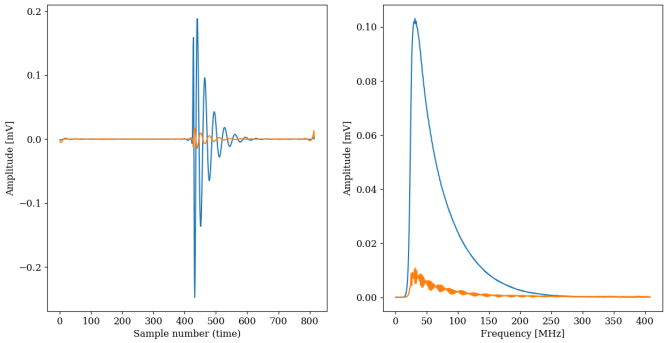

Figure 13: Signal with background from Galactic radio emission added.

A further step would be to investigate how this type of background will affect the measured signal, and whether the better choice is to install narrowband filters or subtract the background in analysis.

Further work should be put into implementing simulation of background from Galactic radio emission. Results derived during this project can be seen in Figure 13. However, the background is not properly normalized, and the plot has been manipulated by multiplying with a constant. The simulation should be improved before implementing it in the ARIANNA detector simulation, making the background simulation of the experiment complete.

Acknowledgements

I would like to thank Anna Nelles for guidance, and also being a great inspiration, throughout the project. Thanks to Timo Krag and other members of the IceCube group for their help and constructive comments along the way. Finally, I would like to thank DESY for the opportunity to do this project, in particular Gernot Maier and Katrin Vaschen for organizing the summer student program at DESY Zeuthen.

References

[1] S.W. Barwick et al. "A first search for cosmogenic neutrinos with the ARIANNA Hexagonal Radio Array". In: *Astroparticle Physics* 70 (2015), pp. 12–26. ISSN: 0927-6505. DOI: https://doi.org/10.1016/j.astropartphys.2015.04.002. URL: http://www.sciencedirect.com/science/article/pii/S0927650515000638.

[2] S.W. Barwick et al. "Radio detection of air showers with the ARIANNA experiment on the Ross Ice Shelf". In: *Astroparticle Physics* 90 (2017), pp. 50–68. ISSN: 0927-6505. DOI: https://doi.org/10.1016/j.astropartphys.2017.02.003. URL: http://www.sciencedirect.com/science/article/pii/S0927650516302134.

[3] Anna Nelles. "Recent results from the ARIANNA neutrino experiment". In: *EPJ Web Conf.* 135 (2017), p. 05002. DOI: 10.1051/epjconf/201713505002. arXiv: 1609.07193 [astro-ph.IM].

[4] T. Huege and D. Besson. "Radio-wave detection of ultra-high-energy neutrinos and cosmic rays". In: *Progress of Theoretical and Experimental Physics* 2017.12, 12A106 (Dec. 2017), 12A106. DOI: 10.1093/ptep/ptx009. arXiv: 1701.02987 [astro-ph.IM].

[5] T. Huege, M. Ludwig, and C. W. James. "Simulating radio emission from air showers with CoREAS". In: *AIP Conf. Proc.* 1535 (2013), p. 128. DOI: 10.1063/1.4807534. arXiv: 1301.2132 [astro-ph.HE].

[6] S. Fliescher. "Antenna Devices and Measurement of Radio Emission from Cosmic Ray induced Air Showers at the Pierre Auger Observatory". PhD. RWTH Aachen University.

[7] T. Karsken. "An Absolite Calibration of the Antennas at LOFAR". M.Sc. Radboud Universiteit Nijmegen.

[8] A. Nelles et. al. "NuRadioReco". In: *GitHub repository* (2018). URL: https://github.com/nu-radio/NuRadioReco.